Altered global brain network topology as a trait marker in patients with anorexia nervosa

Daniel Geisler[1], Viola Borchardt[2,3], Ilka Boehm[1], Joseph A. King[1], Friederike I. Tam[1,4], Michael Marxen[5], Ronald Biemann[6], Veit Roessner[4], Martin Walter[2,3,7,8] and Stefan Ehrlich[1,4]

[1]Division of Psychological and Social Medicine and Developmental Neuroscience, Faculty of Medicine, Technische Universität Dresden, Dresden, Germany; [2]Clinical Affective Neuroimaging Laboratory, Magdeburg, Germany; [3]Department of Behavioral Neurology, Leibniz Institute for Neurobiology, Magdeburg, Germany; [4]Department of Child and Adolescent Psychiatry, Eating Disorder Treatment and Research Center, Faculty of Medicine, Technische Universität Dresden, Dresden, Germany; [5]Department of Psychiatry and Neuroimaging Center, Technische Universität Dresden, Dresden, Germany; [6]Institute of Clinical Chemistry and Pathobiochemistry, Otto-von-Guericke University, Magdeburg, Germany; [7]Clinic for Psychiatry and Psychotherapy, Eberhard-Karls University, Tuebingen, Germany and [8]Center for Behavioral Brain Sciences (CBBS), Magdeburg, Germany

Abstract

Background. Resting state functional magnetic resonance imaging studies have identified functional connectivity patterns associated with acute undernutrition in anorexia nervosa (AN), but few have investigated recovered patients. Thus, a trait connectivity profile characteristic of the disorder remains elusive. Using state-of-the-art graph–theoretic methods in acute AN, the authors previously found abnormal global brain network architecture, possibly driven by local network alterations. To disentangle trait from starvation effects, the present study examines network organization in recovered patients.
Methods. Graph–theoretic metrics were used to assess resting-state network properties in a large sample of female patients recovered from AN (recAN, *n* = 55) compared with pairwise age-matched healthy controls (HC, *n* = 55).
Results. Indicative of an altered global network structure, recAN showed increased assortativity and reduced global clustering as well as small-worldness compared with HC, while no group differences at an intermediate or local network level were evident. However, using support-vector classifier on local metrics, recAN and HC could be separated with an accuracy of 70.4%.
Conclusions. This pattern of results suggests that long-term recovered patients have an aberrant global brain network configuration, similar to acutely underweight patients. While the finding of increased assortativity may represent a trait marker of AN, the remaining findings could be seen as a scar following prolonged undernutrition.

Introduction

Anorexia nervosa (AN) is an eating disorder characterized by an intense fear of weight gain despite severe emaciation caused by self-starvation. Affected individuals typically deny the severity of the disorder, which often leads to protracted course and high mortality (Steinhausen, 2002). Although the underlying mechanisms are unknown, biological underpinnings including genetic heritability are widely recognized (Kaye *et al.*, 2013). Previous studies investigating cortical gray matter reported sizeable and relatively global atrophic changes during acute illness (King *et al.*, 2018). However, along with a number of endocrine changes (Merle *et al.*, 2011; Schorr and Miller, 2017), this (pseudo)atrophy has been found to be largely reversible after successful nutritional therapy (King *et al.*, 2015; Bernardoni *et al.*, 2016).

Studies using task-based functional magnetic resonance imaging (fMRI) in AN have employed a broad range of psychological paradigms, but most have focused on eating disorder-related stimuli (e.g. food and body images). Results suggest alterations in brain regions related to reward processing (Fladung *et al.*, 2010; Cowdrey *et al.*, 2011; Holsen *et al.*, 2012; Decker *et al.*, 2015; Wierenga *et al.*, 2015) and cognitive control (Foerde *et al.*, 2015). However, findings are inconsistent with regard to the direction and precise localization of functional anomalies due to varying-task designs, performance levels, and statistical modeling.

A valuable approach to circumvent some of these inconsistencies may be resting state functional connectivity (RSFC) analysis. Since RSFC data are obtained while the participant is not engaged in a task, some of the aforementioned challenges are eliminated. Hence, RSFC provides a reliable means to study clinical populations with a large variance in compliance. Studies employing this approach have typically used independent component analysis (ICA) or seed-based connectivity analyses to examine known networks such as the default-mode

network (Greicius *et al.*, 2003), the cognitive-control network (Cole and Schneider, 2007) or the salience network (Seeley *et al.*, 2007).

Previous work has demonstrated widespread cortical (Cowdrey *et al.*, 2014), limbic (Favaro *et al.*, 2014) as well as cortico-limbic (Biezonski *et al.*, 2016) dysconnectivities in acute AN. Studies employing ICA found hyper- and hypo-connectivity in the fronto-parietal 'control' network (Gaudio *et al.*, 2016), default-mode (Cowdrey *et al.*, 2011; Boehm *et al.*, 2014), and the somato-sensory and visual networks (Favaro *et al.*, 2012). Recent studies using a seed-based approach identified alterations in thalamo-prefrontal (Biezonski *et al.*, 2016) and ventral fronto-parietal connectivity (Collantoni *et al.*, 2016). However, despite an increase of RSFC studies in AN (Gaudio *et al.*, 2016), the number of studies is still small in comparison with other psychiatric disorders. Furthermore, most studies have focused on acutely underweight patients and thus may have merely measured unspecific effects of starvation (Gaudio *et al.*, 2016).

Going beyond simple focus on synchronous activity of specific brain regions or components of interest, graph–theoretical techniques model the brain's architecture as a complex network (Bullmore and Sporns, 2009; Fornito *et al.*, 2017). Graph theory describes the brain as a set of nodes (representing brain areas or voxels across the whole brain) connected by edges (interregional functional connections) (Bullmore and Bassett, 2011; Fornito *et al.*, 2017). In contrast to conventional RSFC approaches, a representation as a graph provides insight into both regional and whole-brain scales by means of metrics including efficiency of information transfer, small-world topology, and modularity (Rubinov and Sporns, 2010).

We previously applied this data-driven approach in a relatively large sample of acutely ill patients with AN (Ehrlich *et al.*, 2015; Geisler *et al.*, 2016), focusing on global, intermediate, and local brain network properties and using well-established graph metrics as well as Network Based Statistics (NBS, Zalesky *et al.*, 2010). We found that the network structure in acute AN is characterized by increases in both, characteristic path length and global assortativity and by changes in intermediate brain architecture driven by locally decreased connectivity strength and increased path length in posterior insula and thalamus. Our findings obtained in underweight AN patients within the first days of treatment, are suggestive of wide-scale disturbances in information flow across brain networks. It is currently unclear, however, whether these aberrant network properties are a state marker related to undernutrition (such as endocrine changes) or whether they reflect a predisposition which could serve as a biomarker.

Studying patients recovered from AN (recAN) can help to resolve this ambiguity (state *v.* trait marker) since effects would be unrelated to acute undernutrition. Given prior evidence that the assessment of global network properties are reliable, these parameters should be sensitive to uncover either no differences in brain network topology between recAN and matched healthy controls (HC) (indicative of a state-related phenomenon) or differences that resemble our previous findings in acute AN (suggestive of a trait marker).

Materials and methods

Participants

Two independent groups of female volunteers were investigated: 55 recovered former AN patients and pairwise matched 55 female HC (15.5–29.5 years old).

To be considered 'recovered', recAN subjects had to (i) have previously met AN criteria [based on Diagnostic and Statistical Manual of Mental Disorders (DSM)-IV], (ii) maintain a body mass index (BMI) >10th BMI percentile (if <18 years) or a BMI > 18.5 kg/m^2 (if ⩾18 years) for at least 6 months prior to the study, (iii) menstruate, and (iv) have not binged, purged, or engaged in significant restrictive eating patterns. To be included in the HC group, participants had to be of normal weight and eumenorrheic. This study was approved by the local Institutional Review Board, and all participants (or their legal guardians) gave written informed consent. Case–control age-matching was carried out resulting in a maximum difference of 0.6 years between the individuals within one pair (online Supplementary material 1.1).

Exclusion criteria and possible confounding variables, e.g. the use of psychotropic medications other than selective serotonin reuptake inhibitor (SSRI) (two recAN) and medical comorbidities, were obtained using the expert version of the structured interview for anorexia and bulimia nervosa for DSM-IV (SIAB-EX) and our own semi-structured research interview. HC participants did not have any history of psychiatric illness or a lifetime BMI below the 10th age percentile (if <18 years)/BMI below 18.5 kg/m^2 (if ⩾18 years) (online Supplementary material 1.1).

Clinical measures

Eating disorder-specific psychopathology was assessed with the Eating Disorders Inventory (EDI-2). Depressive symptoms were explored using the Beck Depression Inventory (BDI-2). General psychopathology was gaged using the revised Symptom Checklist 90 (SCL-90-R). See online Supplementary material 1.1 for further details. Additionally, plasma leptin was sampled (online Supplementary material 1.2).

MRI data acquisition

Images were acquired between 8 and 9 am after an overnight fast using standard sequences with a 3T MRI scanner (TRIO; Siemens, Erlangen, Germany) using a 12-channel head coil.

Functional images were acquired at rest with eyes closed using a gradient-echo T2*-weighted echo planar imaging (EPI) sequence: tilted 17° toward coronal from the AC–PC line (to reduce signal dropout in orbitofrontal regions); number of volumes = 190; number of slices = 40; TR = 2200 ms; TE = 30 ms; flip angle = 75°; 3.4 mm in-plane resolution; slice thickness = 2.4 mm (1 mm gap resulting in a voxel size of $3.4 \times 3.4 \times 3.4$ mm^3); FoV = 220×220 mm^2; bandwidth = 2004 Hz/pixel, length = 6:58 min (online Supplementary material 1.3).

MRI data preprocessing

MRI images were processed using SPM8 (http://www.fil.ion.ucl.ac.uk/spm/) within the Nipype framework (Gorgolewski *et al.*, 2011). A sample-specific template was created using structural images from all participants. The slice time corrected functional data were realigned and registered to their mean. The realigned files were coregistered to the participant's structural brain image. The EPI volumes were then normalized to MNI space using the sample-specific template and corresponding flow field. Using DPARSFA toolbox, temporal filtering (0.01–0.08 Hz) was applied. Then, regression of 5 CompCorr nuisance components from white matter and cerebrospinal fluid, and of 24 motion

parameters was performed. Subsequently, scrubbing was applied to eliminate timepoints with a framewise displacement of >0.5 mm (Power *et al.*, 2012). The resulting volumes were parcellated into 160 spherical regions of interest (ROIs) as defined by Dosenbach *et al.* (2010). Time courses of these ROIs were extracted and symmetric correlation matrices with pair-wise Pearson correlation coefficients were created. See online Supplementary material 1.4 for further details.

Computation of graph metrics

Based on correlation matrices, weighted, undirected graph networks with 160 nodes were constructed on individual subject level. The distributions of all Pearson correlation coefficients from correlation matrices [which have been shown to drive differences in higher level graph theoretical measures in other neuropsychiatric disorders (van den Heuvel *et al.*, 2017)] were not different across groups (online Supplementary material Fig. S1). Graphs were thresholded with 21 sparsity levels (10–30%, online Supplementary material 1.4). Network metrics were derived using functions from the open-source python library networkx (https://networkx.github.io). Global graph metrics describe the whole network in a single measure, while local graph metrics characterize each node individually.

The five global metrics clustering coefficient (CC_{glob}), characteristic pathlength (CPL_{glob}), small-worldness index (σ), assortativity (α), and global efficiency (E_{glob}), as well as eight local graph metrics degree, strength, local characteristic pathlength (CPL_{loc}), betweenness centrality (BCI), participation index (PI), local efficiency (E_{loc}), local clustering coefficient (CC_{loc}), and normalized local efficiency ($LEGE$) were computed for each sparsity level. For a detailed description of local and global graph metrics, see online Supplementary material 1.5 and 1.6.

Statistical analysis

In all statistical analyses we used age-adjusted BMI standard deviation scores (BMI-SDS; online Supplementary material 1.7). A Shapiro–Wilk test revealed that all graph metrics were not normally distributed. Therefore, non-parametric independent two-group Mann–Whitney U tests were performed for between-group comparisons using the R toolbox (online Supplementary material 1.7).

If our previous findings of group differences in global assortativity and pathlength in acAN (Geisler *et al.*, 2016) constitute trait characteristics of the disorder, we expected to find a similar pattern of results in recAN. For the remaining global metrics test results were corrected for multiple comparisons using false discovery rate (FDR, $p = 0.05$).

For local metrics, we hypothesized group differences (Geisler *et al.*, 2016) in characteristic pathlength (CPL_{loc}) in the left mid-insula, left post-insula, bilateral thalamus, and in strength in the left thalamus, left mid-insula, and left post-insula. For the remaining variables, test statistics were corrected for multiple comparisons across all regions and local metrics (FDR, $p < 0.05$). FDR correction was not applied when comparing the results of networks constructed with different sparsity threshold levels, as they are deemed to be highly interdependent.

To transform the sparsity threshold dependent values of the global metrics into threshold-independent values, we calculated the area-under-the-curve (AUC) of the threshold levels (10–30%) and the corresponding values of the global and local metrics.

Correlative relationships of metrics showing significant group differences with clinical and demographic parameters were assessed using AUC metrics. We focused on overall eating disorder symptoms (EDI-2 total score), depression (BDI-2 total score), BMI-SDS, plasma leptin level, duration of illness, and age. To account for possibly confounding effects of age and BMI-SDS, additional partial correlation analyses were carried out. Results of the correlation analyses were Bonferroni-corrected for 18 comparisons.

Network-based statistics

NBS is a validated method for identifying a statistically significant cluster of connections indicating differences between two groups on intermediate network scales (Zalesky *et al.*, 2010).

NBS are computed using the following steps: (i) identify all connections (pairs of nodes) that are different between groups beyond a particular *t*-value (called *primary threshold*), (ii) select the largest contiguous cluster of these connections, and (iii) validate the cluster's significance by permutation testing. In permutation testing an empirical null distribution of the largest cluster size is generated by conducting the first two NBS steps on resampled group membership data 5000 times. The returned subnetwork is statistically significant at a family wise error (FWE) corrected value of $p < 0.05$. Although the network needs to be considered as a whole, the extent of the returned network can be varied using a different primary threshold. As described previously, we used a primary threshold of $t = 2.0$ (Geisler *et al.*, 2016). This adjusts the extremity of deviation in a connection between groups required, before it is considered for inclusion in the NBS result. NBS returns a single *p*-value, which represents the likelihood that the subnetwork is due to a true effect in the data. This approach measures the entire cluster of returned connections, but does not identify the contribution of each connection independently. The NBS procedure was carried out twice with one-sided *t* tests for the contrasts recAN < HC and recAN > HC.

Machine learning approach

To discriminate between recAN and HC, a linear support vector classifier (SVC) was applied to the AUC-values of the all eight local metrics (degree, strength, CPL_{loc}, BCI, PI, E_{loc}, CC_{loc}, $LEGE$) of all 160 regions.

Based on a set of training data, an SVC computes a hyperplane that separates the data optimally according to a particular cost function in an attempt to find a decision boundary that generalizes the classification for unseen participants (Gunn, 1998). In detail, a classifier is derived by providing examples of the form $\langle x, c \rangle$ to find a hyperplane that best separates the input space, where x represents the input data (e.g. AUC values of eight local metrics for the 160 brain regions) and c is the class label (in this case diagnostic group, recAN $= -1$, HC $= 1$). Computation of the SVC was carried out using the open-source python library scikit-learn (Pedregosa *et al.*, 2011). A standard linear SVC kernel, L2 regularization, and a regularization strength parameter $C = 1$ were employed.

We used a stratified *k*-fold cross-validation strategy to estimate the generalization ability of our classifier, i.e. the classification accuracy in independent test data. We used $k = 10$, corresponding to 11 subjects per fold. In stratified *k*-fold cross-validation, the data is randomly split into *k* folds of equally distributed patient and control cases. A model is trained using $k - 1$ of the folds

Table 1. Basic demographic and clinical variables

	HC		recAN			
	Mean	S.D.	Mean	S.D.	T	
Age (years)	22.4	3.3	22.4	3.3	−0.10	
BMI	21.7	2.1	20.7	1.7	2.80	**
BMI SDS	−0.2	0.7	−0.5	0.5	2.94	**
Minimal lifetime BMI	20.1	1.9	14.3	1.5	17.10	***
IQ	109.7	9.3	110.8	10.2	−0.59	
Handedness score	0.2	0.4	0.1	0.4	0.24	
EDI-2 total score	17.1	3.5	21.5	6.3	−4.52	***
SCL-90-R GSI	0.3	0.4	0.5	0.4	−2.29	*
BDI- total score	4.6	5.5	8.9	8.5	−3.14	**
Leptin, g/ml	14.3	10.0	9.8	6.0	1.54	**

BMI, body mass index; BMI SDS, age-adjusted BMI standard deviation scores; EDI-2, eating disorder inventory, version 2; BDI-2, Beck depression inventory, version 2; SCL-90-R GSI, revised symptom checklist 90 global symptom score, S.D., standard deviation.

Handedness score ranges from 0 (right) to 2 (left). For details on the assessment of IQ and handedness see online Supplementary material 1.1 and 1.2. Group differences were tested using Student's *t* tests.

80% of the recAN participants were predominately of the restrictive subtype and 20% were predominately of the binge/purge subtype during acute illness as ascertained with the SIAB-EX interview.

*$p < 0.05$, **$p < 0.01$, ***$p < 0.001$.

and its generalization performance was validated on the remaining fold. This process is repeated k times, each time withholding a different validation subset. The average classification accuracy over all k models represents the overall generalizability.

We used permutation tests to non-parametrically evaluate the null hypothesis that the classifiers might have obtained good classification accuracies just by chance (Ojala and Garriga, 2010). This involved repeating the classification procedure 3000 times with a different random permutation of the training group labels.

Results

Sample characteristics

There were no differences in age, intelligence quotient (IQ), or handedness score between the groups. RecAN had as expected lower minimal lifetime BMI, slightly lower current BMI and plasma leptin levels, as well as residual eating disorder symptom and depression scores (Table 1).

Topological properties (global metrics)

We first tested differences between recAN and HC in assortativity (α) and characteristic pathlength (CPL_{glob}). The groups did not differ in pathlength, but recAN had a higher assortativity for 19 of 21 tested sparsity thresholds with p-values between 0.02 and 0.05 (Fig. 1).

Next, we tested for group differences in the remaining global graph measures small-worldness index (σ), clustering-coefficient (CC_{glob}), and global efficiency (E_{glob}). After correcting for multiple comparisons, both small-worldness index and clustering-coefficient were reduced in recAN (Fig. 1). In all tested sparsity thresholds, group comparisons yielded p-values (FDR corrected) between 0.008 and 0.044.

Group comparisons using AUC values and FDR over all five measures confirmed significant differences for assortativity,

small-worldness index, and clustering-coefficient ($W = 1131$, $p_{FDR} = 0.031$; $W = 1950$, $p_{FDR} = 0.031$; $W = 1992$, $p_{FDR} < 0.025$), but no differences for the remaining metrics. All group differences remained significant after excluding the two recAN taking SSRI ($W = 1050$, $p_{FDR} = 0.029$; $W = 1814$, $p_{FDR} = 0.029$; $W = 1857$, $p_{FDR} < 0.029$).

Neither assortativity, small-worldness index nor clustering-coefficient were associated with age, BMI, or plasma leptin in either group (all $|r| < 0.23$ and $p_{FDR} > 0.64$). There were also no correlations between these metrics and eating disorder (EDI-2 total score) or depressive symptoms (BDI-2 total score; all $|r| < 0.35$ and $p_{FDR} > 0.26$). The absence of significant correlations was confirmed when controlling for age or BMI (all $|r| < 0.35$ and $p_{FDR} > 0.26$).

Network-based statistics

No differences in subnetworks were found between recAN and HC.

Nodal characteristics (local metrics)

For the nodal characteristics tested within our hypothesis-driven approach [characteristic pathlength (CPL_{loc}) and strength], we did not find any group differences (online Supplementary material Fig. S2). Group comparisons of the remaining local graph metrics were also not significant after correction for multiple comparisons (eight metrics). Visual inspection of the uncorrected findings (online Supplementary material Figs. S3–S13) revealed a pattern of relatively consistent trends toward group differences predominantly in fronto-parietal brain regions for the measures degree, strength, local efficiency (E_{loc}), and normalized local efficiency ($LEGE$). Therefore, a SVC was trained on the nodal characteristics to discriminate between recAN and HC as an exploratory analysis. The SVC reached a classification score of 70.4%, which is significantly above chance with $p = 0.0003$
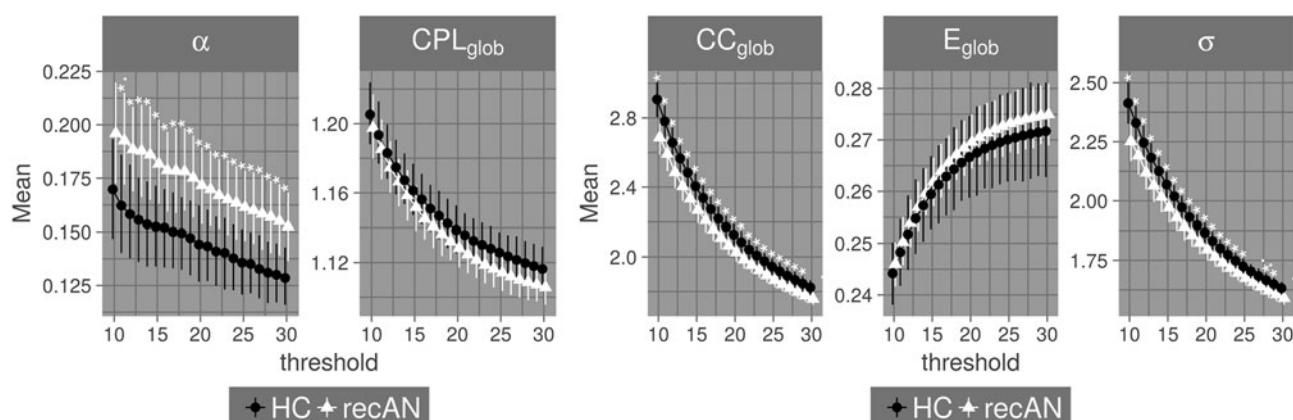
Fig. 1. Group comparisons of global metrics. Results of group comparison of the global metrics characteristic pathlength (CPL_{glob}), assortativity (α), clustering-coefficient (CC_{glob}), global efficiency (E_{glob}) and small-worldness index (σ) for all tested sparsity thresholds between 10 and 30. Comparisons were performed using Mann–Whitney U tests ($**p < 0.01$; $*p < 0.5$; $\cdot p < 0.1$). According to our a priori hypothesis, p-values for CPL_{glob} and α were uncorrected, whereas p-values for CC_{glob}, E_{glob}, and σ were FDR-corrected for multiple comparisons. HC and recovered AN patients (recAN) are depicted by black circles and white triangles, respectively. Group comparisons using AUC values and FDR over all five measures confirmed significant differences for assortativity, small-worldness index, and clustering-coefficient.
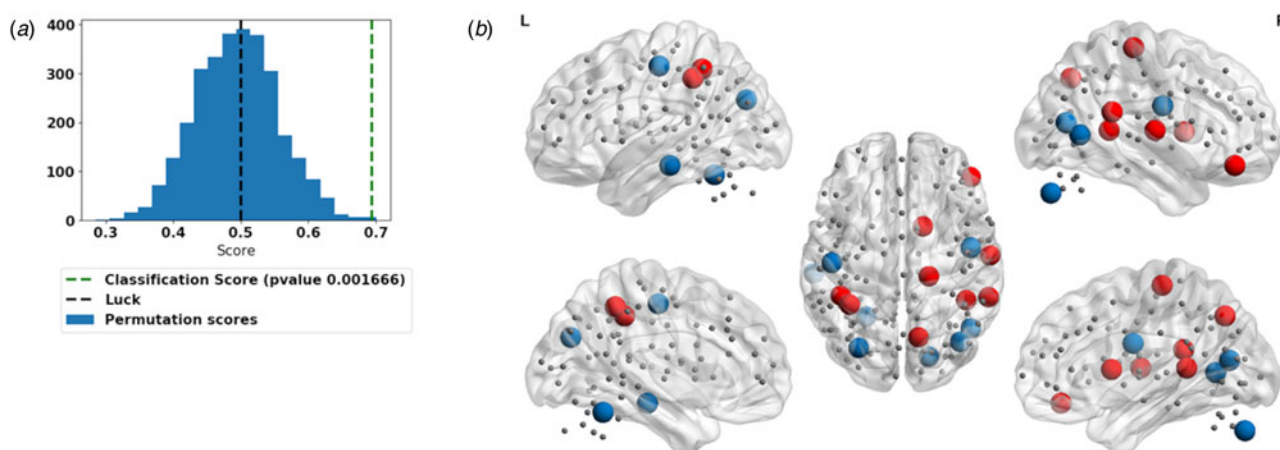

Fig. 2. Machine learning approach. (*a*) Results of the support vector classifier (SVC) using all local graph metrics to determine group membership: histogram of classification scores based on the permutated (blue bars) and actual (green) samples using SVCs. Classification score represents the accuracy of the classifier and are estimated as the ratio of correct classified test labels to the total number of test labels. (*b*) Localization of SVC features: only the regions of features with the highest positive and lowest negative weights are shown (according to Table 2). Red and blue colors indicate positive and negative weights, respectively.

(Fig. 2*a*). Classification appeared to be driven by differences in several local graph metrics in temporo-parietal brain regions (Table 2 and Fig. 2*b*).

Discussion

The current study demonstrates changes in the configuration of large-scale functional brain networks of recovered AN patients for the first time using graph–theoretical metrics of RSFC. We found that the global functional network structure of recovered patients is characterized by an increased assortativity representing an affinity for nodes of a similar degree to connect directly with each other – a result that mirrors changes in acutely underweight AN patients (Geisler *et al.*, 2016). This finding suggests increased assortativity as a trait and possible biomarker for AN. Furthermore, recAN were characterized by a reduced CC_{glob}, reflecting diffuse reduced local connectedness, and a decreased small-worldness index. The latter findings can be interpreted as a tendency toward a more 'random' network structure.

In contrast to acute AN, we did not find significant changes in the CPL_{glob}, or in graph metrics at the intermediate (NBS, Ehrlich *et al.*, 2015) or local level (Geisler *et al.*, 2016). However, beyond group-level differences, a SVC was able to distinguish recAN from HC individuals based on local graph metrics with a classification accuracy of 70.4%, driven by degree and *BCI* in predominantly parietal and temporal brain regions.

At the global level, the pattern of functional brain network connectivity observed previously in acAN (Geisler *et al.*, 2016) and here in recAN seems to be characterized by high-degree nodes that preferentially connect to other high-degree nodes (Newman, 2002). At the same time, this increased assortativity in AN reflects propensity of low degree nodes to preferentially connect to other low degree nodes (Fig. 3). Conjointly, this configuration of highly interconnected hub nodes as well as specialized clusters of low-degree nodes is suggestive of a trait reflecting altered global network topology in the disorder. Such a configuration has been described as 'cost-efficient' (Achard and Bullmore, 2007). However, after approximating the distance

Table 2. Features of support vector classifier (SVC)

	SVC coefficient	Mean HC	Mean recAN
10 most positive features			
Postparietal_L_99__betweenness_centrality	0.0333	0.002	0.0016
Parietal_R_74__PI	0.0294	0.1184	0.1026
Temporal_R_95__PI	0.0291	0.1017	0.0936
Precuneus_R_132__strength	0.028	3.0558	2.5717
vlPFC_R_15__degree	0.0276	5.0699	3.5507
Temporal_R_95__E_loc	0.0274	0.1406	0.1369
IPL_L_88__E_loc	0.0273	0.1531	0.1482
Parietal_R_89__l_cc_real	0.0271	0.0444	0.0397
Temporal_R_60__degree	0.0268	10.391	10.1385
Basalganglia_R_39__betweenness_centrality	0.0266	0.0014	0.001
10 most negative features			
Parietal_L_64__degree	−0.0236	5.3724	7.0131
Inftemporal_L_72__E_loc	−0.0249	0.1508	0.1549
Latcerebellum_L_109__degree	−0.0256	6.1397	6.7845
Infcerebellum_R_155__strength	−0.0256	2.0152	2.4208
Temporal_R_123__betweenness_centrality	−0.0266	0.001	0.0014
Occipital_L_142__degree	−0.0291	6.9087	8.115
Infcerebellum_R_155__degree	−0.0292	4.7181	5.6317
Occipital_R_135__betweenness_centrality	−0.034	0.0007	0.0008
Precentralgyrus_R_51__betweenness_centrality	−0.0352	0.0003	0.0006
Latcerebellum_L_109__betweenness_centrality	−0.0388	0.0013	0.0019

Only the features with the highest positive and lowest negative weights are listed. For the sake of completeness the group means of the raw feature values are provided as well. In the SVC the groups recAN and HC were coded by −1 and 1, respectively. The name of the features consists of the ROI identifier (anatomical name, hemisphere, and unique index number) and the name of the local metric. For more details regarding the ROIs, please refer to online Supplementary material Table S2

(Euclidean distance) between nodes and comparing the mean lengths of connections between the groups, there were no significant differences ($W = 1686$, $p = 0.23$) indicating that the network configurations of recAN participants and HC have comparable costs. Increased assortativity may also pose a risk since network efficiency can be reduced greatly by degradation of high-degree nodes. Hence, networks characterized by high assortativity may be less robust (van den Heuvel and Sporns, 2011).

Furthermore, compared with the HC, the global brain network architecture in recAN seems to have a subtle randomization of the small-world pattern with a reduced connectivity between node neighbors. This pattern has been previously reported in schizophrenia (Lynall *et al.*, 2010) and obsessive compulsive disorder (Armstrong *et al.*, 2016). Cabral *et al.* (2012) modeled the influence of an aberrant structural connectivity on the functional connectivity. They discovered that structural dysconnection may result in a network reorganization characterized by a decrease in both small-worldness and clustering. Gray matter volume reductions are pronounced in acute AN, but largely reversible with weight restoration – suggestive of a state-effect (Wagner *et al.*, 2006; King *et al.*, 2015; Bernardoni *et al.*, 2016). However, findings on white matter microstructure are more heterogeneous (Pfuhl *et al.*, 2016; Vogel *et al.*, 2016; King *et al.*, 2018). Remnants of structural dysconnectivity in recAN, which may not be

detectable using standard DTI sequences, could potentially also explain differences in global functional network structure.

Changes in assortativity were also found in acutely underweight AN patients (Geisler *et al.*, 2016). An exploratory comparison (Fig. 3) of recAN and acute AN patients included in our previous study (Geisler *et al.*, 2016) indicates that recovering from AN is accompanied by a moderate decrease in assortativity – but assortativity is still higher than in HC. An (exploratory) follow-up analysis attempting to unravel the type of brain regions which drive the increase in assortativity revealed subtle group differences in local assortativity (which did not withstand our rigorous control for multiple testing) in nine predominantly occipital and parietal brain regions (see online Supplementary material Table S3). These additional findings suggest a global effect based on small changes in distributed brain areas. Since none of the group differences found in the current sample were related to age, BMI, depressive symptoms, eating disorder symptoms or leptin levels, also when controlling for age and BMI, it seems possible that hyper-assortativity represents a trait effect rather than a state effect of AN. Trait effects are assumed to be relatively independent of undernutrition (and other variables closely related to acute illness) and may function as predisposing factors. If confirmed, e.g. in subclinical samples, increased assortativity could potentially also serve as a biomarker which could help to identify
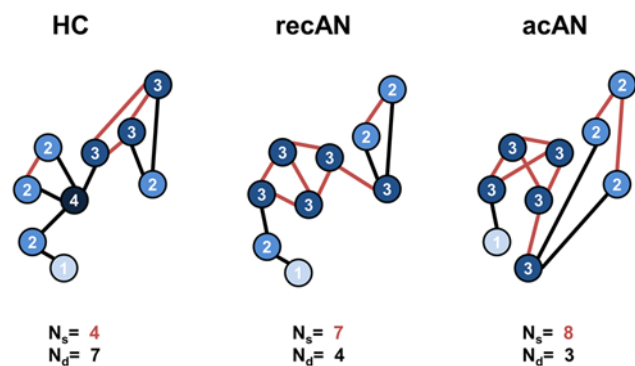
Fig. 3. Schematic representation of assortativity in brain network topology of HC and patients with anorexia nervosa. Nodes are labeled by their degree. If an edge connects nodes of the same degree, it is colored red; otherwise it is colored black. N_S (same degree) and N_d (different degree) denote the numbers of red and black edges of the whole graph, respectively. Positive assortativity: high-degree nodes primarily connect to other high-degree nodes and low-degree nodes connect to other low-degree nodes. All three topological architectures presented above showed positive assortativity. However, assortativity increases from healthy participants to recAN to acutely ill AN (acAN). We found this pattern of increase in the actual data. An exploratory analysis on the AUC assortativity values confirmed significantly higher values in recAN (mean$_{AUC}$ = 3.45, s.d.$_{AUC}$ = 1.39) if compared with the acute patients (mean$_{AUC}$ = 4.23, s.d.$_{AUC}$ = 1.84; n = 35; W = 1278, p = 0.01) included in our previous study (Geisler et al., 2016). HC showed the lowest assortativity (mean$_{AUC}$ = 2.90, s.d.$_{AUC}$ = 1.27) that was significantly different from recAN (W = 1131, p_{FDR} = 0.031, see results section). See online Supplementary material 1.8 for more details.

at-risk individuals or tailor early interventions and treatment intensity.

In contrast, for the reductions in small-worldness index and CC, which were not (yet) observed in young (and mostly first-episode) underweight AN patients, an explanation that is centered on 'scar' effects from e.g. a prolonged phase of acute illness (and chronic undernutrition) seems equally plausible.

Unlike our previous studies in acutely ill patients where we showed reduced synchronization (Ehrlich et al., 2015) and network efficiency (Geisler et al., 2016) in a thalamo-insular network, the current analyses of intermediate and local network characteristics in recAN showed no group differences after correcting for multiple comparisons. When considering the results before correction for multiple comparisons, however, nominally significant group differences seemed to follow a fronto-parietal pattern. However, a recent methodological study in AN (Lord et al., 2016) suggested that global graph metrics can be interpreted relatively confidently, while local findings may be more dependent on brain parcellation methods and need to be considered more carefully.

While potential biomarkers for a disorder are usually statistically significant at the group level, the discriminative ability of findings on an individual level are typically not evaluated (Arbabshirani et al., 2017). Here, we appraised the diagnostic relevance of local graph metrics by predicting group membership using an SVC. The successful classification was driven by degree and BCI in parietal and temporal brain regions. The found discrimination accuracies of 70.4% is comparable with average accuracy levels in RSFC studies predicting group membership in other neuropsychiatric disorders (Arbabshirani et al., 2017).

Our findings of altered global network topology extend previous results of more traditional RSFC studies in AN which focused on circumscribed networks or a few seed regions. However, a recent integrated review of RSFC studies in AN demonstrates that alterations of functional connectivity cannot be restricted to a few brain regions or networks (Gaudio et al., 2016). In detail, previous studies

in acutely ill patients have shown altered RSFC in widely distributed regions of the brain, such as between the dorsal anterior cingulate cortex and the precuneus, the inferior frontal gyrus, parts of the ventral attention network, and within the somato-sensory network. Moreover, alterations do not seem to be limited to the neocortex, but also occur between subcortical and cortical regions, namely between the thalamus and the dlPFC (Biezonski et al., 2016) as well as between insula and ventral striatum (Frank et al., 2016). Apart from our previous studies, only two other known reports in AN using somewhat comparable local metrics exists (Kullmann et al., 2014; Gaudio et al., 2018). Results of these studies (conducted in acutely underweight AN) suggested reduced degree centrality (the sum of weights of significant connections for a voxel) in the inferior frontal gyrus and reduced connectivity in a subnetwork involved in somatosensory and interoceptive information processing.

Only a small number of studies have examined RSFC in weight-recovered AN patients. Results suggest that some alterations in functional connectivity in the fronto-parietal (Boehm et al., 2016), the default mode (Cowdrey et al., 2014), and the somato-sensory network (Favaro et al., 2012) may persist after recovery. One previous study applied a graph–theoretical analysis approach to white matter tractography data (Zhang et al., 2016) and found abnormal modular structural organization in the form of shifted frontostriatal and fronto-cingulate coupling in weight-restored patients. Although these findings may be seen as complementary, future studies including AN patients at different stages of their illness as well as longitudinal studies are warranted.

Limitations

When considering our work, some important limitations have to be taken into account. First, as properties of graph networks also depend on the chosen brain parcellation and preprocessing algorithm (Fornito et al., 2017), the current results are not independent from the chosen processing pipeline – even though we followed the current standards in the field. This standard analysis also neglects to capture dynamic changes in network configurations and only takes positive edge weights into account. There is increasing evidence suggesting the importance of negative correlations within brain networks of individuals with psychological symptoms (Castellanos et al., 2008; Fox et al., 2009; Whitfield-Gabrieli and Ford, 2012). Second, the cross-sectional nature of the study does not allow differentiation between a true trait marker or a possible scar effect of the disorder regarding the observed differences in brain network architecture in recAN. To clarify whether those neural substrates are a consequence or a potential precursor of pathologic eating behavior, future longitudinal studies are needed. Third, the results of the study are limited to the brain function at rest and the specific metrics investigated. Further investigations of trait-level reconfiguration during task performance and using other metrics such as modularity could provide a deeper understanding of the neurobiological processes (Vatansever et al., 2015). Fourth, although our samples were meticulously age-matched, effects of age on network configurations cannot be ruled out entirely. However, the large and homogeneous sample consisting of relatively young and almost exclusively unmedicated recAN may be viewed as a strength of our study.

Conclusion

The current study, which is the largest RSFC study in recAN to date, provides evidence for altered global brain network

architecture in recovered AN patients, indicating a wide-scale disturbance in information flow across brain networks. Of note, a configuration in which high degree nodes are preferentially connected with similar high degree nodes and vice versa seems to characterize patients with acute as well as recovered AN, suggestive of a trait that may predispose to the illness or an early effect of undernutrition that does not normalize with recovery. Our findings provide new insights into the neurobiology underlying this disorder by providing support for an 'altered global network architecture' perspective. Furthermore, this study is a large step toward better predictive ability to classify patients at an individual level using brain-based biomarkers which potentially could help diagnosing AN early and may guide the selection and timing of treatments.

References

Achard S and Bullmore E (2007) Efficiency and cost of economical brain functional networks. *PLoS Computational Biology* **3**, e17.

Arbabshirani MR, Plis S, Sui J and Calhoun VD (2017) Single subject prediction of brain disorders in neuroimaging: promises and pitfalls. *NeuroImage* **145**, 137–165.

Armstrong CC, Moody TD, Feusner JD, McCracken JT, Chang S, Levitt JG, Piacentini JC and O'Neill J (2016) Graph-theoretical analysis of resting-state fMRI in pediatric obsessive-compulsive disorder. *Journal of Affective Disorders* **193**, 175–184.

Bernardoni F, King JA, Geisler D, Stein E, Jaite C, Nätsch D, Tam FI, Boehm I, Seidel M, Roessner V and Ehrlich S (2016) Weight restoration therapy rapidly reverses cortical thinning in anorexia nervosa: a longitudinal study. *NeuroImage* **130**, 214–222.

Biezonski D, Cha J, Steinglass J and Posner J (2016) Evidence for thalamo-cortical circuit abnormalities and associated cognitive dysfunctions in underweight individuals with anorexia nervosa. *Neuropsychopharmacology* **41**, 1560–1568.

Boehm I, Geisler D, King JA, Ritschel F, Seidel M, Deza Araujo Y, Petermann J, Lohmeier H, Weiss J, Walter M, Roessner V and Ehrlich S (2014) Increased resting state functional connectivity in the fronto-parietal and default mode network in anorexia nervosa. *Frontiers in Behavioral Neuroscience* **8**, 346.

Boehm I, Geisler D, Tam F, King JA, Ritschel F, Seidel M, Bernardoni F, Murr J, Goschke T, Calhoun VD, Roessner V and Ehrlich S (2016) Partially restored resting-state functional connectivity in women recovered from anorexia nervosa. *Journal of Psychiatry & Neuroscience: JPN* **41**, 377–385.

Bullmore E and Sporns O (2009) Complex brain networks: graph theoretical analysis of structural and functional systems. *Nature reviews. Neuroscience* **10**, 186–198.

Bullmore ET and Bassett DS (2011) Brain graphs: graphical models of the human brain connectome. *Annual Review of Clinical Psychology* **7**, 113–140.

Cabral J, Hugues E, Kringelbach ML and Deco G (2012) Modeling the outcome of structural disconnection on resting-state functional connectivity. *NeuroImage* **62**, 1342–1353.

Castellanos FX, Margulies DS, Kelly C, Uddin LQ, Ghaffari M, Kirsch A, Shaw D, Shehzad Z, Di Martino A, Biswal B, Sonuga-Barke EJS, Rotrosen J, Adler LA and Milham MP (2008) Cingulate-precuneus interactions: a new locus of dysfunction in adult attention-deficit/hyperactivity disorder. *Biological Psychiatry* **63**, 332–337.

Cole MW and Schneider W (2007) The cognitive control network: integrated cortical regions with dissociable functions. *NeuroImage* **37**, 343–360.

Collantoni E, Michelon S, Tenconi E, Degortes D, Titton F, Manara R, Clementi M, Pinato C, Forzan M, Cassina M, Santonastaso P and Favaro A (2016) Functional connectivity correlates of response inhibition impairment in anorexia nervosa. *Psychiatry Research* **247**, 9–16.

Cowdrey FA, Park RJ, Harmer CJ and McCabe C (2011) Increased neural processing of rewarding and aversive food stimuli in recovered anorexia nervosa. *Biological Psychiatry* **70**, 736–743.

Cowdrey FA, Filippini N, Park RJ, Smith SM and McCabe C (2014) Increased resting state functional connectivity in the default mode network in recovered anorexia nervosa. *Human Brain Mapping* **35**, 483–491.

Decker JH, Figner B and Steinglass JE (2015) On weight and waiting: delay discounting in anorexia nervosa pretreatment and posttreatment. *Biological Psychiatry* **78**, 606–614.

Dosenbach NUF, Nardos B, Cohen AL, Fair DA, Power JD, Church JA, Nelson SM, Wig GS, Vogel AC, Lessov-Schlaggar CN, Barnes KA, Dubis JW, Feczko E, Coalson RS, Pruett JR, Barch DM, Petersen SE and Schlaggar BL (2010) Prediction of individual brain maturity using fMRI. *Science (New York, N.Y.)* **329**, 1358–1361.

Ehrlich S, Lord AR, Geisler D, Borchardt V, Boehm I, Seidel M, Ritschel F, Schulze A, King JA, Weidner K, Roessner V and Walter M (2015) Reduced functional connectivity in the thalamo-insular subnetwork in patients with acute anorexia nervosa. *Human Brain Mapping* **36**, 1772–1781.

Favaro A, Santonastaso P, Manara R, Bosello R, Bommarito G, Tenconi E and Di Salle F (2012) Disruption of visuospatial and somatosensory functional connectivity in anorexia nervosa. *Biological Psychiatry* **72**, 864–870.

Favaro A, Tenconi E, Degortes D, Manara R and Santonastaso P (2014) Effects of obstetric complications on volume and functional connectivity of striatum in anorexia nervosa patients. *The International Journal of Eating Disorders* **47**, 686–695.

Fladung A-K, Grön G, Grammer K, Herrnberger B, Schilly E, Grasteit S, Wolf RC, Walter H and von Wietersheim J (2010) A neural signature of anorexia nervosa in the ventral striatal reward system. *The American Journal of Psychiatry* **167**, 206–212.

Foerde K, Steinglass JE, Shohamy D and Walsh BT (2015) Neural mechanisms supporting maladaptive food choices in anorexia nervosa. *Nature Neuroscience* **18**, 1571–1573.

Fornito A, Bullmore ET and Zalesky A (2017) Opportunities and challenges for psychiatry in the connectomic era. *Biological Psychiatry: Cognitive Neuroscience and Neuroimaging* **2**, 9–19.

Fox MD, Zhang D, Snyder AZ and Raichle ME (2009) The global signal and observed anticorrelated resting state brain networks. *Journal of Neurophysiology* **101**, 3270–3283.

Frank GKW, Shott ME, Riederer J and Pryor TL (2016) Altered structural and effective connectivity in anorexia and bulimia nervosa in circuits that regulate energy and reward homeostasis. *Translational Psychiatry* **6**, e932.

Gaudio S, Wiemerslage L, Brooks SJ and Schiöth HB (2016) A systematic review of resting-state functional-MRI studies in anorexia nervosa: evidence

for functional connectivity impairment in cognitive control and visuospatial and body-signal integration. *Neuroscience and Biobehavioral Reviews* **71**, 578–589.

Gaudio S, Olivo G, Beomonte Zobel B and Schiöth HB (2018) Altered cerebellar-insular-parietal-cingular subnetwork in adolescents in the earliest stages of anorexia nervosa: a network-based statistic analysis. *Translational Psychiatry* **8**, 127.

Geisler D, Borchardt V, Lord AR, Boehm I, Ritschel F, Zwipp J, Clas S, King JA, Wolff-Stephan S, Roessner V, Walter M and Ehrlich S (2016) Abnormal functional global and local brain connectivity in female patients with anorexia nervosa. *Journal of Psychiatry & Neuroscience: JPN* **41**, 6–15.

Gorgolewski K, Burns CD, Madison C, Clark D, Halchenko YO, Waskom ML and Ghosh SS (2011) Nipype: a flexible, lightweight and extensible neuroimaging data processing framework in python. *Frontiers in Neuroinformatics* **5**, 13.

Greicius MD, Krasnow B, Reiss AL and Menon V (2003) Functional connectivity in the resting brain: a network analysis of the default mode hypothesis. *Proceedings of the National Academy of Sciences of the United States of America* **100**, 253–258.

Gunn SR (1998) *Support Vector Machines for Classification and Regression.* Technical Report no. 14. Southampton: School of Electronics and Computer Science, pp. 85–86.

Holsen LM, Lawson EA, Blum J, Ko E, Makris N, Fazeli PK, Klibanski A and Goldstein JM (2012) Food motivation circuitry hypoactivation related to hedonic and nonhedonic aspects of hunger and satiety in women with active anorexia nervosa and weight-restored women with anorexia nervosa. *Journal of Psychiatry & Neuroscience: JPN* **37**, 322–332.

Kaye WH, Wierenga CE, Bailer UF, Simmons AN and Bischoff-Grethe A (2013) Nothing tastes as good as skinny feels: the neurobiology of anorexia nervosa. *Trends in Neurosciences* **36**, 110–120.

King JA, Geisler D, Ritschel F, Boehm I, Seidel M, Roschinski B, Soltwedel L, Zwipp J, Pfuhl G, Marxen M, Roessner V and Ehrlich S (2015) Global cortical thinning in acute anorexia nervosa normalizes following long-term weight restoration. *Biological Psychiatry* **77**, 624–632.

King JA, Frank GKW, Thompson PM and Ehrlich S (2018) Structural neuroimaging of anorexia nervosa: future directions in the quest for mechanisms underlying dynamic alterations. *Biological Psychiatry* **83**, 224–234.

Kullmann S, Giel KE, Teufel M, Thiel A, Zipfel S and Preissl H (2014) Aberrant network integrity of the inferior frontal cortex in women with anorexia nervosa. *NeuroImage: Clinical* **4**, 615–622.

Lord A, Ehrlich S, Borchardt V, Geisler D, Seidel M, Huber S, Murr J and Walter M (2016) Brain parcellation choice affects disease-related topology differences increasingly from global to local network levels. *Psychiatry Research* **249**, 12–19.

Lynall M-E, Bassett DS, Kerwin R, McKenna PJ, Kitzbichler M, Muller U and Bullmore E (2010) Functional connectivity and brain networks in schizophrenia. *The Journal of Neuroscience* **30**, 9477–9487.

Merle JV, Haas V, Burghardt R, Döhler N, Schneider N, Lehmkuhl U and Ehrlich S (2011) Agouti-related protein in patients with acute and weight-restored anorexia nervosa. *Psychological Medicine* **41**, 2183–2192.

Newman MEJ (2002) Assortative mixing in networks. *Physical Review Letters* **89**, 208701.

Ojala M and Garriga GC (2010) Permutation tests for studying classifier performance. *Journal of Machine Learning Research* **11**, 1833–1863.

Pedregosa F, Varoquaux G, Gramfort A, Michel V, Thirion B, Grisel O, Blondel M, Prettenhofer P, Weiss R and Dubourg V and others (2011). Scikit-learn: machine learning in python. *Journal of Machine Learning Research* **12**, 2825–2830.

Pfuhl G, King JA, Geisler D, Roschinski B, Ritschel F, Seidel M, Bernardoni F, Müller DK, White T, Roessner V and Ehrlich S (2016) Preserved white matter microstructure in young patients with anorexia nervosa? *Human Brain Mapping* **37**, 4069–4083.

Power JD, Barnes KA, Snyder AZ, Schlaggar BL and Petersen SE (2012) Spurious but systematic correlations in functional connectivity MRI networks arise from subject motion. *NeuroImage* **59**, 2142–2154.

Rubinov M and Sporns O (2010) Complex network measures of brain connectivity: uses and interpretations. *NeuroImage* **52**, 1059–1069.

Schorr M and Miller KK (2017) The endocrine manifestations of anorexia nervosa: mechanisms and management. *Nature Reviews Endocrinology* **13**, 174–186.

Seeley WW, Menon V, Schatzberg AF, Keller J, Glover GH, Kenna H, Reiss AL and Greicius MD (2007) Dissociable intrinsic connectivity networks for salience processing and executive control. *The Journal of Neuroscience* **27**, 2349–2356.

Steinhausen H-C (2002) The outcome of anorexia nervosa in the 20th century. *The American Journal of Psychiatry* **159**, 1284–1293.

van den Heuvel MP and Sporns O (2011) Rich-club organization of the human connectome. *The Journal of Neuroscience* **31**, 15775–15786.

van den Heuvel MP, de Lange SC, Zalesky A, Seguin C, Yeo BTT and Schmidt R (2017) Proportional thresholding in resting-state fMRI functional connectivity networks and consequences for patient-control connectome studies: issues and recommendations. *NeuroImage* **152**, 437–449.

Vatansever D, Menon DK, Manktelow AE, Sahakian BJ and Stamatakis EA (2015) Default mode dynamics for global functional integration. *The Journal of Neuroscience* **35**, 15254–15262.

Vogel K, Timmers I, Kumar V, Nickl-Jockschat T, Bastiani M, Roebroek A, Herpertz-Dahlmann B, Konrad K, Goebel R and Seitz J (2016) White matter microstructural changes in adolescent anorexia nervosa including an exploratory longitudinal study. *NeuroImage: Clinical* **11**, 614–621.

Wagner A, Greer P, Bailer UF, Frank GK, Henry SE, Putnam K, Meltzer CC, Ziolko SK, Hoge J, McConaha C and Kaye WH (2006) Normal brain tissue volumes after long-term recovery in anorexia and bulimia nervosa. *Biological Psychiatry* **59**, 291–293.

Whitfield-Gabrieli S and Ford JM (2012) Default mode network activity and connectivity in psychopathology. *Annual Review of Clinical Psychology* **8**, 49–76.

Wierenga CE, Bischoff-Grethe A, Melrose AJ, Irvine Z, Torres L, Bailer UF, Simmons A, Fudge JL, McClure SM, Ely A and Kaye WH (2015) Hunger does not motivate reward in women remitted from anorexia nervosa. *Biological Psychiatry* **77**, 642–652.

Zalesky A, Fornito A and Bullmore ET (2010) Network-based statistic: identifying differences in brain networks. *NeuroImage* **53**, 1197–1207.

Zhang A, Leow A, Zhan L, GadElkarim J, Moody T, Khalsa S, Strober M and Feusner JD (2016) Brain connectome modularity in weight-restored anorexia nervosa and body dysmorphic disorder. *Psychological Medicine* **46**, 2785–2797.